IOSR Journal of Applied Chemistry (IOSR-JAC)
e-ISSN: 2278-5736.Volume 17, Issue 1 Ser. I (January 2024), PP 01-11
www.iosrjournals.org

Water and Energy Sustainability via Thermoresponsive Hygroscopic Acrylamide Gel: Synthesis and Water Release Kinetics

Nasrollah Hamidi*[1], Mehrdad Yazdani-Pedram[2], Donald Walter[1], John B. Willams[1]

[1]*Department of Biological and Physical Sciences/1890-Research, South Carolina State University, Orangeburg, SC 29117 USA.*

[2]*Facultad de Ciencias Químicas Y Farmacéuticos, Universidad de Chile, Santiago, Chile*

Abstract

This study reports on the synthesis, characterization, and water release kinetics of a sample of deliquescent acrylamide hydrogel imbibed in activated carbon powder using thermal analysis and FT-IR spectroscopy. It was synthesized by the radical polymerization of acrylamide and N, N'-methylene-bis-acrylamide in the presence of potassium persulfate, calcium chloride, and activated carbon powder. The kinetics of water desorption were evaluated with a pseudo-single component model applied to the isoconversional method using thermogravimetric analysis (TGA) thermograms at heating rates ranging from 0.25 to 8.0 Kmin^{-1}. The highest water release rate at 0.25 Kmin^{-1} was at 39 °C, a temperature easily achievable through sunlight photo-thermal heating. All extents of reaction (α) were fit best for diffusional models, except for a few that matched better with power type models. The $\mathbf{E_a}$ *for water release was found to be approximately 23 kJmole^{-1}, which is lower than the vaporization energy of water (46 kJmole^{-1}). The differential scanning calorimetry (DSC) thermogram showed a transition centered at 25 °C, which is close to the maximum water release rate of TGA. Therefore, its phase transition from hydrophilic to hydrophobic caused water release, a phenomenon that has been confirmed by other researchers and makes the product suitable as a condenser for passive atmospheric water generators.*

Keywords: *atmospheric water harvesting, hydrogel, freshwater, desiccants, thermoresponsive gel*

Date of Submission: 26-12-2023 Date of Acceptance: 06-01-2024

I. INTRODUCTION

This investigation focused on the preparation, steam absorption, and water desorption of a poly(acrylamide) hydrogel sample imbibed in $CaCl_2$, as a co-water absorbent and activated carbon powder as a solar energy harvester. It was studied using thermogravimetric analysis (TGA), differential scanning calorimetry (DSC), and attenuated total reflectance Fourier transform infrared (ATR-FTIR) spectroscopy techniques. This research is significant because it tackles the issue of generating water from the atmosphere to counter the impacts of climate change on the availability of clean water. Hygroscopic salt and acrylamide gels show promising results for extracting water from the environment.[1,2] This strategy has the potential for the development of passive atmospheric water generation (AWG) technologies.[3]

The Earth has 1,386 million cubic kilometers of water, however, only 35.5 million cubic kilometers (2.5%) is freshwater, and less than 0.75% of this freshwater is sustainably managed. Human activity and climatic change are causing freshwater resources to decline, making water anxiety the fifth leading global risk.[4–9] Worldwide, the consumption of potable water tripled within the last 50 years.[6,10,11] Another consumer of freshwater is the agricultural and food production industry which withdraws over 74% of freshwater, and a 14% increase in this figure is predicted by 2030.[12–14] Moreover, mineral contamination is a fundamental problem in many regions, such as in the 50 countries located in the Pacific Ring of Fire.[15] However, water desalination[16,17] could alleviate water stress for more than four billion people [18] who live near saline water resources.[14,19] In some arid and humid areas of Asia, America, and Africa, AWG technologies collecting fog, rain, and vapor have been installed to alleviate local water stress and prevent poverty and forced relocation.[3,20,21] Freshwater anxiety could be widely relieved by developing AWG technologies to harvest renewable, invisible atmospheric vapor, which is estimated to be equivalent to 12,900 cubic kilometers of liquid water.[22,23] The availability of individual AWG

*Corresponding author, nhamidi@scsu.edu

units operating by the force of nature (i.e. passive AWGs) would relieve pressure on power resources, and many water-stressed situations independent of geo-climatic conditions.

The amount of vapor in the air (~ 1-3%) [24] is measured as the percent of relative humidity (% RH), and its concentration depends on the location, time, temperature, and geographic and climatic conditions. [23,25] A cool atmosphere holds less moisture, about 7% less per one degree (1°C) of cooling than a warm one. Temperature variations during the day and night cause changes in the air's relative humidity, producing dewfall as a natural water source for plants and animals, in arid and humid regions, in particular. Dewfall is also used for human consumption as AWG technologies become more popular.[26] Active AWG technologies require significant energy input and result in substantial heat release, and their mechanisms are more thermodynamically complicated than passive AWG technologies or fog harvesters that work with the forces of nature.[1,27–30]

The emergence of temperature-responsive polymers that regulate water condensation and release at the molecular level by transitioning from hydrophilic to hydrophobic by temperature changes has increased the successful development of AWG technologies.[31–35] When they are placed in an interpenetrating polymeric gel network, they capture moisture from the air at lower temperatures and release water via a phase separation process at a slightly higher temperature. Poly(acrylamide),[1] poly(N-vinyl caprolactone),[36] poly(N,N-diethylamino ethyl methacrylate), poly(pyrrole chloride) (PPy-Cl),[37] poly(N-isopropylacrylamide) (PNIPAM),[31,38] and some copolymers such as poly(L-lactic acid)−poly-(ethylene glycol)−poly(L-lactic acid) are among those stimuli-responsive polymers.[31,39,40] Their behavior has inspired the creation of responsive nanostructured polymer materials and systems in the forms of thin films, particulates, and assemblies to harvest environmental water. Smart materials isolation or in a network of hygroscopic minerals and polymers have provided good moisture absorption and desorption networks.[41–43] The hydrogel becomes hygroscopic [44] with the addition of sorbents such as salts,[1] metal−organic frameworks,[45] or hygroscopic polymers.[34] Generally, three processes co-occur inside the hydrogel: vapor transport, sorption, and liquid transport.[46] Vapor transport through interconnected gaseous micropores relies on diffusion due to the presence of a vapor pressure difference. Sorption occurs on the liquid−gas interface of the micropores. In the intervening time, the liquid is transported through the nanopores of the polymer network, driven by the water chemical potential difference between the wet and dry regions of the polymer network.[47] The redistribution of water leads to the structural change of micropores and polymer networks and further induces a volumetric expansion of the hydrogel due to the pore elastic effect.[33] This effect is unique to hydrogels compared to other commonly used sorbent systems with rigid materials.[24]

PNIPAM undergoes a phase transition at its lower critical solution temperature (LCST) near 32 °C.[31,38] Hair-size fibers made of a mixture of hydrophobic plastics with hydrophilic PNIPAM capture water from a highly humid atmosphere at lower temperatures (below 25 °C) within a few minutes and released it at above 35 °C.[38] The amount of thermoresponsive PNIPAM at the skin layer controlled the wettability of the fibers. Other hydrophilic polymers, such as nylon, have also given good results when electro-sprayed on the surface of the fibers to condense dewfall. Also, a combination of PNIPAM with hydrophilic sodium alginate made an interpenetrating polymer network gel that can capture moisture from the air and directly extract liquid water.[3,31,40,41]

Metal-organic frameworks (MOFs) resulting from reticular chemistry are another kind of three-dimensional interconnected network of highly porous crystalline solid materials suitable for AWGs fabrication. [24,42,43] The desorption process requires heat input depending on the water molecules' adsorption strength to reach regeneration temperature, which varies from 70 -170 °C.[29,48]

Hygroscopic minerals such as calcium chloride, lithium chloride, lithium bromide, silica gel, and zeolite attract moisture everywhere in very low and highly humid environments. [3,49–53] These moisture absorbents have been used to fabricate AWGs that harvest moisture at night when the air humidity increases by natural cooling of the warm air. The water desorption occurred during the day by heating the hygroscopic bed with solar radiation in a closed container.[3] For example, in a dry and arid region experiencing a 20% RH at 30 °C during the day, an energy-intensive and impractical process must cool the air to below its dew point (~ < 4 °C) to turn vapor into liquid. However, by heating the humid descants, air humidity reaches above 80% RH at 30 °C in the cabin, and then the vapor liquefied at temperatures below the dew point (below 26 °C). This process requires less energy than extracting water from dry air in arid environments.[54–56]

In our quest for searching for new materials for the construction of AWGs, an acrylamide hydrogel containing $CaCl_2$ as an effective water absorbing, activated carbon powder as a source of radiation energy absorbent, and an acrylamide hydrogel as the frame for the system and water regulator, where it accumulates water at the hydrophilic state and release waster at its hydrophobic state was prepared and submerged to TGA experimentation. Six water desorption thermograms at heating rates ranging from 0.25 to 8.0 $Kmin^{-1}$, which are attainable under solar radiation, were performed and analyzed to understand the accurate mechanism of its water desorption. The maximum rate of water release was estimated at each thermogram by its derivative. The TGA thermograms and their derivatives were analyzed based on the isoconversional method [32,57–59] to estimate the

kinetics triplet for water desorption at the temperature range of 30-120 °C. The obtained values were within expectations and supported the funding in the published literature.

II. EXPERIMENTAL

Materials

Activated carbon powder, acrylamide (AA), calcium chloride ($CaCl_2$), N, N'-methylene bis acrylamide (MBAA), and potassium persulfate were purchased from Fisher Scientific, a Thermo Fischer Scientific (USA) company. They were used as received. Fresh distilled water was prepared in the lab.

Synthesis

Five (5.0) g of distilled water, 21 mg of activated carbon powder as solar heat absorbent, and 4.02 g $CaCl_2$ were added to a 60 mL ThermoScientific™ screwed cap septum vial. The mixture was dispersed by exposure to ultrasound for 2 hours. Then 922 mg of AA, 4.4 mg of MBAA as a crosslinking agent, 1.4 mg of potassium persulfate as the polymerization initiator, were added to the mixture and shaken to dissolve. The mixture was held for 45 min under a stream of 20 $mLmin^{-1}$ ultrapure argon to eliminate the oxygen present then on top of a hot plate at ~70 °C untill gel formation was completed. The product (CDAAG) was a black uniform AA hydrogel embedded with activated carbon powder and $CaCl_2$, as shown in picture 1. Six pieces of the gel were cut for the study.

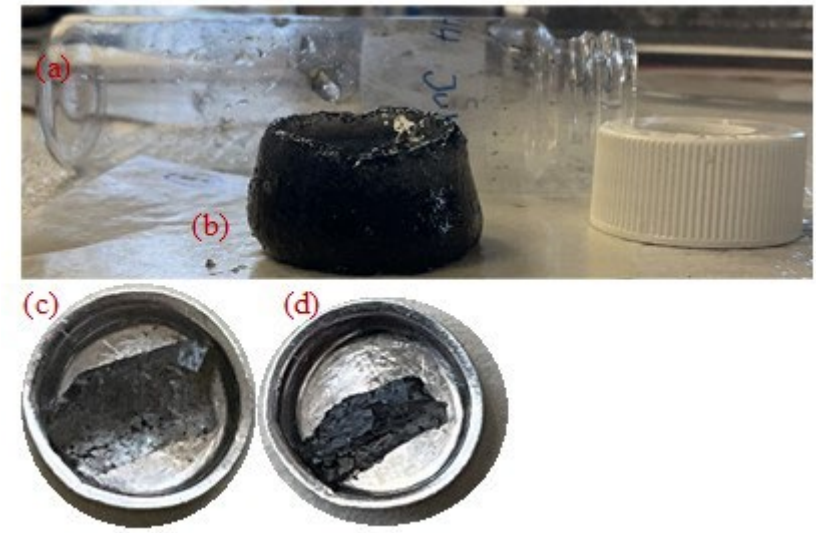

Picture 1. (a) the polymerization container and its cap; (b) the CDAAG after removal from botel; (c) a cut of gel in TGA pan saturated with water before heating; (d) the sample after scanned with β = 0.25 $Kmin^{-1}$ to 120 °C.

Thermal Analysis

Thermogravimetric Analysis (TGA)

The TGA studies were conducted on a TGA-7 Thermogravimetric Analyzer (PerkinElmer, Inc., USA) run by a Dell PC using Pyrus 13.2.3. It was calibrated by four-points calibration method since the thermocouple in this device is not in direct contact with the sample. The absorption reaction was prevented by increasing temperature linearly and a well-controlled nitrogen stream of 60 $mLmin^{-1}$ (room temperature and pressure), which carried the volatiles away as soon as they formed. The sample weight preserved was recorded continuously with the corresponding temperature and time. Six scans were carried out at the rates of 0.25, 0.5, 1, 2, 4, and 8 $Kmin^{-1}$ to evaluate the kinetics parameters accurately. The data were downloaded to Microsoft Excel for the study.

The values of the extent of desorption (α) for each sample were estimated by (%W1-%Wi)/(%W1-%Wf) where %W1 represents the initial weight percent of the sample, usually 100%, %Wi represents the weight percent of the remaining sample at any time, and %Wf = 55.44% represents the %W of the sample at the end of the dehydration process based on thermograms at the heating rates of 0.25 and 0.50 $Kmin^{-1}$. The values of α increased from zero to one as the dehydration progressed from initiation to completion for the scans at 0.25, 0.50, and 1.0 $Kmin^{-1}$, respectively and they were lower for the other samples that the dehydration was not completed.

Differential Scanning Calorimetry (DSC)

The DSC experiments were carried out on a DSC-7 Differential Scanning Calorimeter (PerkinElmer, Inc., USA) under a continuous stream of 60 $mLmin^{-1}$ of argon, operated by a Dell PC using Pyrus 13.2.3. The instrument was calibrated using a standard sample of indium. A piece of gel (40 mg) was inserted into a stainless-steel liquid DSC pan for thermal analysis. The DSC cell was chilled to -30 °C before running the sample.

Attenuated total reflectance Fourier transform infrared (ATR-FTIR) spectroscopy

We employed a Perkin-Elmer (USA) FT-IR Spectrophotometer, specifically the Spectrum Two model, which was outfitted with a PerkinElmer ATR (ATR-FTIR) accessory. This instrument operated using the Spectrum IR program version 10.6.2 and was controlled via an HP computer. Our aim was to assess the spectroscopic properties of both the reactants and products under ambient conditions. Subsequently, the spectral data were acquired and exported in Excel format for ease of subsequent analysis.

Theory of the kinetics of water desorption

The kinetics of the thermally simulated water release of the CDAAG was studied by the measurement and parameterization of the rates of weight loss originating by eq.1:[59]

$$CDAAG(active) \xrightarrow{\Delta} CDAAG + H_2O\ (vapor) \qquad (1)$$

Moist CDAAG(active) was heated ($\xrightarrow{\Delta}$) to release the absorbed humidity in the form of vapor [H_2O (vapor)] or nano-droplets of water that were carried away with the stream of nitrogen gas (wind). The rate of thermally stimulated dehydration of CDAAG (-dW/dt) was expressed by the negative derivative of TGA thermogram (-DTGA). The rate of dehydration was parameterized by the advancement of dehydration (α), where (1-α) represents the residual amount of water in the sample. The mechanism of the water release is expressed by a pre-assuming kinetic function, $f(\alpha)$, as shown in Table 1. We assumed, that the rate constant follows the Arrhenius relationship [$k(T) = AExp\left(-\frac{E_a}{RT}\right)$], as shown by eq. 2: [60,61]

$$Rate = \frac{d(1-\alpha)}{dt} = -k(T)f(\alpha) = -f(\alpha)AExp(-\frac{E_a}{RT}) \quad (2)$$

where T represents the absolute temperature value in K, $\mathbf{E_a}$ represents the energy barrier to release water by the CDAAG, and R = 8.314 J mol^{-1} K^{-1} is the universal gas constant. Equation (2) is the starting point for various differential kinetic methods and applies to any reaction type. The values of $\mathbf{E_a}$, and ln**A**, with the pre-assumed form of $f(\alpha)$ are estimated from the slope and intercept of the Arrhenius plot based on eq. 3, by plotting [lnRate/$f(\alpha)$] = ln k versus 1/T, for a given value of α, as shown by the graphs in Fig. 4.

$$ln\left[-\frac{dw/dt}{f(\alpha)}\right] = ln\, k = ln\left[\frac{\frac{d\alpha}{dt}}{f(\alpha)}\right] = -\frac{\boldsymbol{E_a}}{RT} + ln\boldsymbol{A} \qquad (3)$$

Equation 3 relates the temperature, and rate of weight loss at each interval when it is applied to TGA data. [62,63]

Table 1. Reaction models that were used to describe the thermally stimulated water release of the CDAAG system.

No.	Reaction Model	Code	$f(\alpha)$
1	Power law	P4	$4\alpha^{3/4}$
2	Power law	P3	$3\alpha^{2/3}$
3	Power law	P2	$2\alpha^{1/2}$
4	Power law	P2/3	$2/3\alpha^{-1/2}$
5	One-dimensional diffusion	D1	$1/2\alpha^{-1}$
6	Mampel (first order)	F1	$(1-\alpha)$
7	Avrami–Erofeev	A4	$4(1-\alpha)[-\ln(1-\alpha)]^{3/4}$
8	Avrami–Erofeev	A3	$3(1-\alpha)[-\ln(1-\alpha)]^{2/3}$
9	Avrami–Erofeev	A2	$2(1-\alpha)[-\ln(1-\alpha)]^{1/2}$
10	Three-dimensional diffusion	D3	$3/2(1-\alpha)^{2/3}[1-(1-\alpha)^{1/3}]^{-1}$
11	Contracting sphere	R3	$3(1-\alpha)^{2/3}$
12	Contracting cylinder	R2	$2(1-\alpha)^{1/2}$
13	Two-dimensional diffusion	D2	$[-\ln(1-\alpha)]^{-1}$
14	Random Scission	L2	$2(\alpha^{1/2}-\alpha)$

III. RESULTS AND DISCUSSIONS

ATR-FTIR Spectroscopy.

Figure 1(a) shows the main vibrational characteristics of AA. Antisymmetric and symmetric N-H stretching vibrations in primary amide moiety, at 3348 and 3199 cm^{-1} and its scissoring vibration at 1417 cm^{-1}. The IR absorption band for a carbonyl group in a compound depending on its structure appears between 1650-1850 cm^{-1}. For simple aldehydes and ketones, its stretching vibration has a strong absorption between 1710 and 1740 cm^{-1}. The carbonyl stretching vibration band for saturated aliphatic ketones appears at 1715 cm^{-1}. Conjugation of the C=O bond with a double bond lowers the stretching frequency, hence, the carbonyl stretching vibration of AA is manifested at 1665 cm^{-1}.

The stretching vibration of a carbon-carbon double bond (C=C) is typically observed in the range of 1600-1680 cm^{-1}. The peaks can vary slightly depending on the specific compound and its environment. It is more intense for cis isomers than for trans isomers. Also, terminal olefins show stronger C=C double bond stretching vibrations than internal double bonds. Not all C=C vibrations are IR-active, and sometimes the C=C stretch can be rather small and difficult to see. The IR stretching vibration of the C=C of the acrylamide end group appears at 1609 cm^{-1} since it is in conjugation with the nearby carbonyl group. The IR spectrum of alkenes C-H stretching peaks between 3100 and 3000 cm^{-1} and the C-H wags of alkenes fall between 1000 and 600.

MBAA is a white solid that is used as a cross-linking agent in polyacrylamides. It is mixed with acrylamide to make polyacrylamide gels for use in protein and nucleic acid electrophoresis, and in our case, for atmospheric water absorption and desorption. Its IR stretching vibrations as shown in Fig. 1(b). The vibrational characteristics of MBAA at 3301 for secondary amide, 3063 for sp^2 hydrogen, 2975 for sp^3 hydrogen, carbonyl group at 1657, and carbon double bond at 1627 all in cm^{-1}.

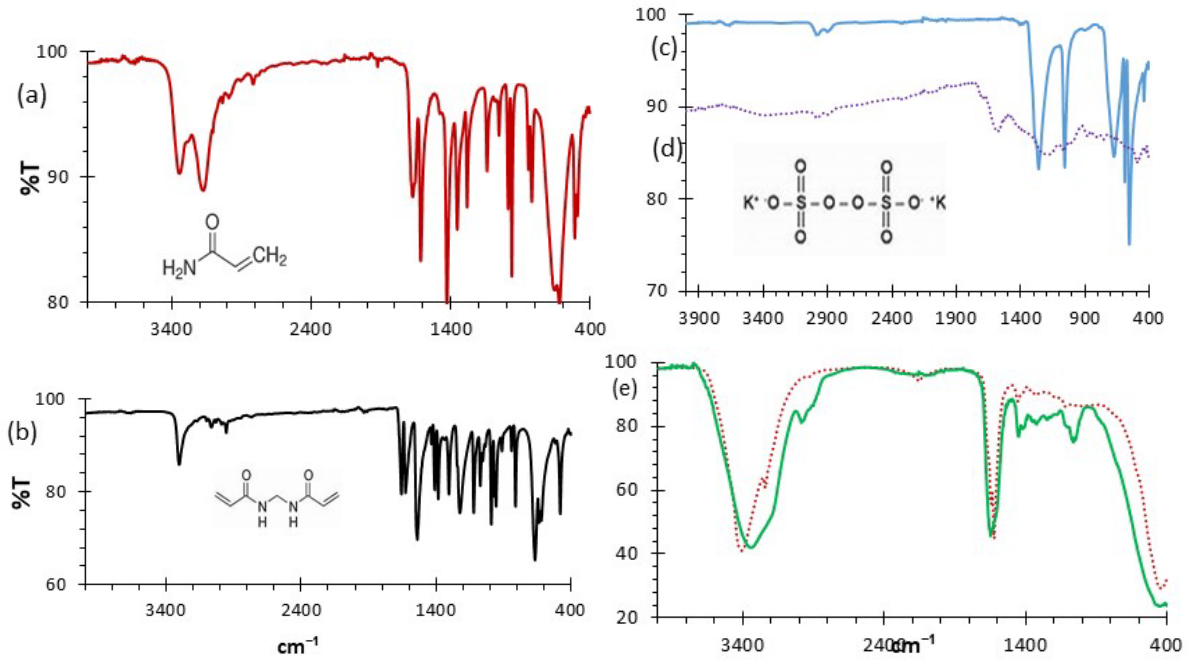

Fig. 1. ATR-FTIR representation of (a) acrylamide, (b) N, N'-bis-methylene-acrylamide, (c) potassium persulfate, (d) activated carbon powder, (e) deliquescent acrylamide hydrogel (CDAAG), (Green wet gel, and red dry gel)

Potassium persulfate has a decomposition temperature of 50-60 °C, ideal for the initiation of radical polymerization in aqueous solutions. Figure 1c shows its IR spectrum with absorption at 1256, 1057, 678, and 556 cm^{-1}.

Figure 1(e) shows the characteristic vibrational properties of CDAAG saturated with water (green full line), the absorptions are centered at 3350 cm^{-1} and a shoulder at 3180 cm^{-1} indicating the presence of primary and secondary amides, combined with the vibration of the hydroxyl group of water. The very weak absorption at 2973 and 2900 cm^{-1} represents the sp^3 hydrogens, and the carbonyl group shifted to 1657 cm^{-1}. The absence of C=C signal indicates the close to complete conversion of reactants to products. The dry hydrogel vibration of N-H and NH_2 are shown at 3356 cm^{-1} and 3161 cm^{-1} and C=O carbonyl at the same place.

Differential Scanning Calorimetry (DSC)

Some industrial applications and the materials' processing types relate to the physical properties of matter, such as melting point (mp) and glass transition temperature (Tg). The relatively high mp (> 300 °C) and Tg temperatures (~163 °C) of polyacrylamide (PAA) result from strong interactions between polar amide groups. During the first DSC scan of the CDAAG as shown in Fig. 2, its physical changes were registered at temperatures ~ 25 °C ($\Delta H \sim 72$ Jg^{-1}, $\Delta C_p \sim 2.4$ $Jg^{-1}K^{-1}$), and Tg ~ 124 °C ($\Delta C_p = 59$ $Jg^{-1}K^{-1}$). These transitions do not coincide with mp (> 300 °C) and Tg (~163 °C) of PAA. Also, they are not related to the AA's mp (84.5 °C). Therefore, they are related to the new product CDAAG, as was expected.

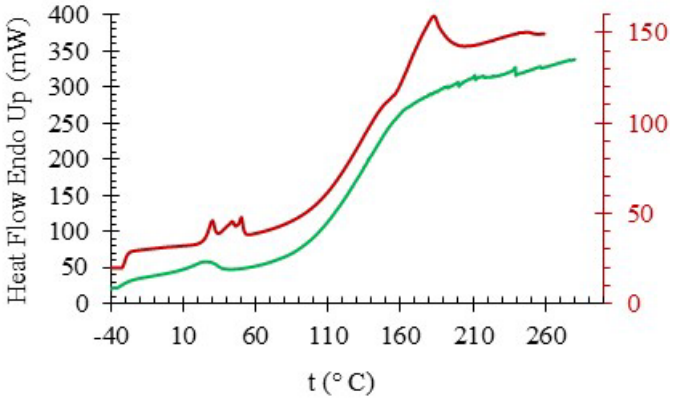

Fig. 2. Differential scanning calorimetry (DSC) thermogram of a sample of CDAAG; 45 mg of wet (green line) at β = 40 $Kmin^{-1}$, and (red line) 33 mg of dry gel at β = 10 $Kmin^{-1}$.

The transition around 25 °C could be related to a phase transition and conformational rearrangements of CDAAG. This thermal transition could also be responsible for the spontaneous release of absorbed vapor in the form of liquid water at temperatures above 40°C as has been supported by other researchers' work.

Thermogravimetry Studies

Six samples CDAAG were analyzed by TGA (Table 2), for water desorption analysis. The weight loss by temperature and time was taken as the measure of water desorption from CDAAG. The variations of normalized weights (%W), advancement of water release (α), and its normalized rates are shown by the graphs in the plots of Fig. *3* (a), (b), (c) and, (d), respectively. The amount of water released depended on time, temperature, and heating rate. For example, at the slower heating rate, β = 0.25 $Kmin^{-1}$, the CDAAG took 121 min to warm up to 60 °C and released about 40% of its absorbed water as shown by the corresponding graph in Fig 3(a) and data in Table 2. While the sample at the faster heating rate, 8 $Kmin^{-1}$, took 5.1 min to reach the same temperature and released 2.5% of its water contents.

Table 2. Water yields (WY, w%) and temperature by heating rates (0.25 to 8 $Kmin^{-1}$) in the temperature range of 40 to 80 °C

β ($Kmin^{-1}$)	m (mg)	40 °C		50 °C		60 °C		70 °C		80 °C	
		WY (%)	t (min)	WY (%)	t (min)	WY (%)	t (min)	WY (%)	t (min)	WY (%)	t (min)
0.25	38.25	21.8	54.8	35.5	88.6	39.7	120.7	41.0	153.7	42.2	184.9
0.50	36.36	15.4	33.3	27.4	54.1	37.2	73.3	39.7	92.4	40.9	107.4
1.0	41.86	7.3	17.2	14.4	27.6	23.0	38.0	31.3	47.8	37.6	56.7
2.0	62.54	2.7	9.0	5.7	14.4	10.0	19.7	15.1	24.7	21.1	29.7
4.0	44.74	1.8	4.6	3.8	7.3	6.6	9.8	10.5	12.4	15.3	14.9
8.0	49.87	0.50	2.5	1.2	3.8	2.5	5.1	4.4	6.4	7.3	8.2

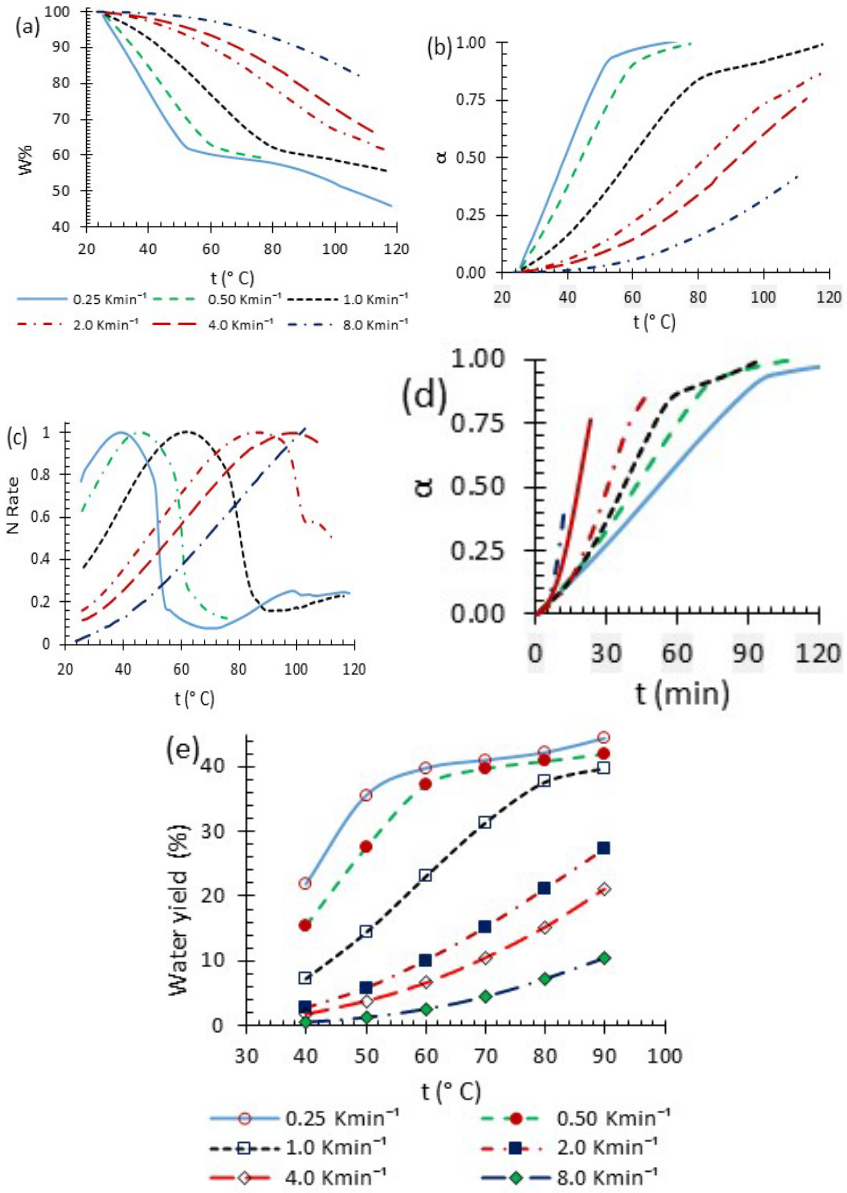

Fig. 3. (a) Thermograms of water desorption, (b) Water desorption advancement, and (c) normalized water desorption rate, (d) α versus time for water release of CDAAG, respectively; and (e) Water yields at a given temperature for a β values.

The water desorption was initiated as soon as the supersaturated sample was placed into the TGA pan (~ 25°C). The yield of water released at a given temperature depended on the heating rates, as can be observed from the data listed in Table 2. As the heating rate, β, was increased, the amounts of water released by the CDAAG at a given temperature were less due to thermal lag effect. For example, at temperature 60 °C, the amount of water released by β = 0.25, 0.50, 1.0, 2.0, 4.0, and 8 $Kmim^{-1}$ were 39.7%, 37.2%, 23.0%, 10.0%, 6.6%, and 2.5%, and the corresponding times are 120.7, 73.3, 38.0, 19.7, 9.8, 5.1 min, respectively, as shown by the data in the corresponding columns of Table 2. This phenomenon indicated the importance of the time factor in warming up CDAAG and providing the time required to change its conformation from the hydrophilic to the hydrophobic phase. Both factors, the thermal lag, and conformational transitions are affecting the amounts of water desorption of CDAAG samples. In this case, the higher heating rate is less effective because of the short duration to reach the indicated temperature.

The tendency of the variation of α and normalized rate of dehydration by temperature as shown in Fig. 3 (b) have the shape of a sigmoid reaction, where the rate of dehydration at the starting point is zero, it increases by the advancement of the dehydration, reaches a maximum and then decreases. For the values of β at 4 and 8 $Kmin^{-1}$, the reaction stopped before completion while the system was in its acceleration to reach its max rate.

Figure 3(d) shows the effects of heating rate on the temperature of the samples, and the amounts of water desorbed at various temperatures and β values. At the β = 0.25 the water desorption plateaus after the sample temperature reaches 60 °C, while at β = 1, the plateau initiates after 90 °C due to thermal lag effects.

The temperature of the maximum rate of water release (R_{max}) also depended on the heating rate, as shown in Fig. *3* (c), and the data listed in Table 3. The maximum rate of water yield was at temperatures below the boiling point of water, ranging from 39 to 98 °C for the β ranging from 0.25 to 4 $Kmin^{-1}$, respectively. Our results were within expectations since other researchers also reported the release of water from acrylamide gels at very low temperatures achievable by photothermal CNTs.[1] Therefore, CDAAG is a good candidate for the condenser fabrication of AWG using passive conditions.

Table 3 shows the values of the maximum rate of water generation (R_{max}, $\%min^{-1}$), temperature at the maximum rate of water generation (T_{max}, °C), and the values of α at the maximum rate of water generation. All maximum values increase with the increasing value of β, indicating the effects of thermal lag on these properties.

Table 3. Variation of the parameters at the maximum water release rate with the heating rate of CDAAG.

β ($Kmin^{-1}$)	R_{max} ($\%min^{-1}$)	T_{max} (°C)	α_{max}	WY (%)
0.25	0.435	39	0.510	20.9
0.50	0.589	45	0.537	22.0
1.0	0.867	62	0.544	24.3
2.0	0.804	86	0.559	24.9
4.0	1.04	98	0.584	26.1

Isoconversional kinetics of water desorption

The plots in Fig. 4 illustrate the relationship between lnk and 1/T, as per the isoconversional model, according to eq. 3, across a range of α values spanning from 0.1 to 0.8. The isoconversional method assumes that the reaction mechanism remains consistent at a specific α value, regardless of the heating rate, and temperature, as referenced by many researchers.[32,60,64–66] This approach was utilized to construct the Arrhenius plot corresponding to the specified α values for dehydration of CDAAG. The slope of the best-fitting line that traverses the data points signifies the value of Ea/R, and the intercept relates to lnA.

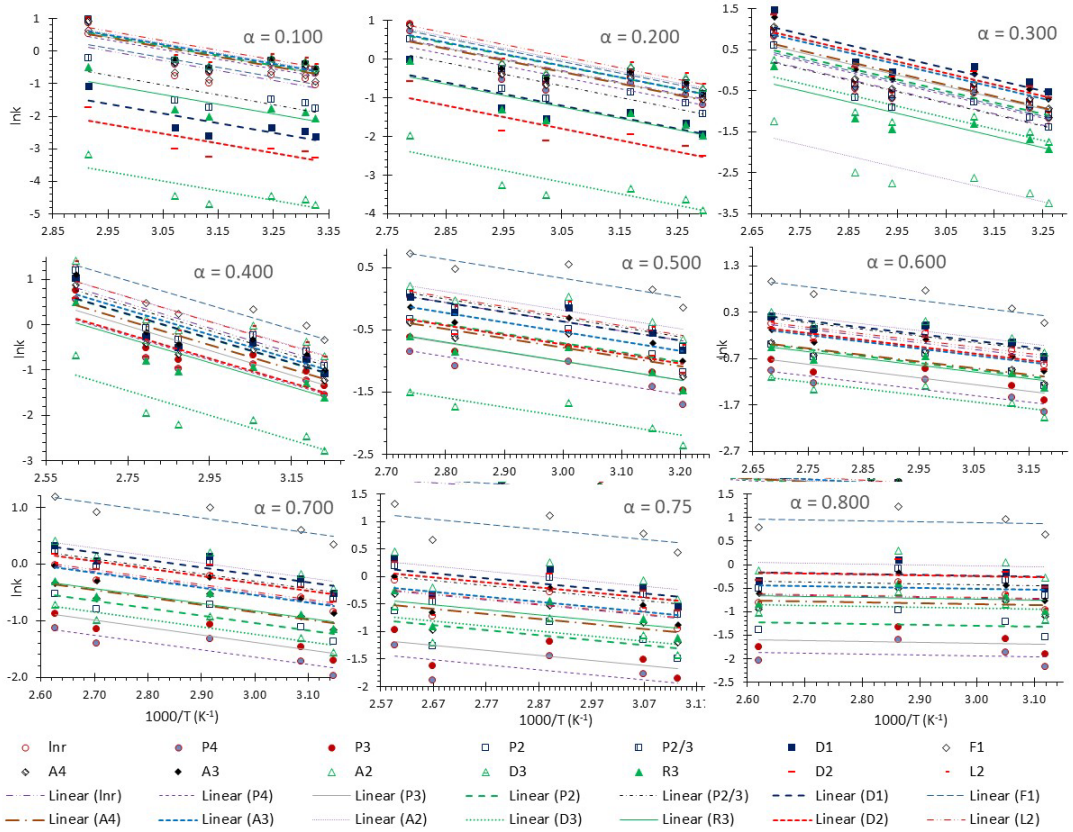

Fig. 4. Arrhenius plots of the CDAAG dehydration at the indicated α values.

For any given α value, the estimated $E_{a,\alpha}$ values obtained from the slopes of the least-squares adjusted lines exhibited proximity, irrespective of the $f(\alpha)$ function. This is evident from the parallel adjusted lines displayed in the plots of Fig. 4, agreeing with the expectations of the method. For instance, considering the case of α = 0.300, the average $E_{a,\,0.300}$ = 23.27 ± 0.03 kJmol^{-1} value derived from the slope of all models, therefore, all the values of $\mathbf{E_a}$ at α = 0.3 superimpose each other as shown in the plot of Fig. *5*(a). However, the values of $\ln A_{0.300}$ = 7.9 ± 0.7 min^{-1} were not coinciding with each other, showing higher values of standard deviation, consequently, as shown in Fig 6(b) where a number of value points were observed for each α value. A similar effect was observed at other extent of water release.

The relative constancy of the values of $\mathbf{E_{a,\alpha}}$ = 23 ± 1 was observed for the α values ranging from 0.05 to 0.4. The values of $\mathbf{E_{a,\alpha}}$ at higher values of α were smaller due to the temperatures above 50 °C which provides higher amounts of energy to release water.

Fig. *5*(a) depicts the variation in energy barrier values ($E_{a,\alpha}$) as determined by the application of the isoconversional method (Eq 3). This is done across a range of α values spanning from 0.050 to 0.80, employing the reaction models enumerated in Table 1. The corresponding lnA values are illustrated in Fig. 5(b), whereas their $\mathbf{r^2}$ values are presented in Fig. 6.

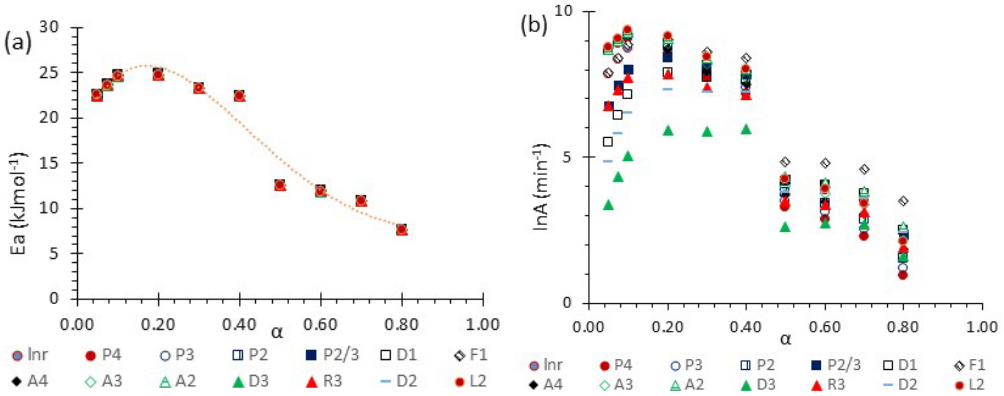

Fig. 5. Variation of (a) activation energy barrier ($E_{a,\alpha}$) and (b) values of Arrhenius pre-exponential factor (lnA) of dehydration of CDAAG versus the corresponding extent of reaction (α), respectively.

Figure 5(b) shows the variation of the values of $\ln\mathbf{A_\alpha}$ by α, as obtained from Arrhenius plots of Fig. 5. The variations of the values of $\ln\mathbf{A_\alpha}$ by α (Fig. 5(b)), show similar tendencies as the variations of $\mathbf{E_{a,\alpha}}$ versus α, disregarding their scattering. It is apparent that the lnA values are influenced by the chosen reaction model, the $f(\alpha)$ function.

The rate of reaction (dα/dt) at a given α value is expressed as the product of two terms, [$\mathbf{A_\alpha}\,f(\alpha)$] and [exp(−$\mathbf{E_\alpha}$/RT)], therefore, as the value of one increases, the two other term has to increase. Comparisons of Figs. 5(a) and (b) show the correlation among $\mathbf{E_{a,\alpha}}$, and $\mathbf{A_\alpha}$. The changes in the values of $\mathbf{A_a}$ related to a given α and $f(\alpha)$ value reflect the change of the mechanism of the individual step of the reaction, which is related to changes in the rate-limiting steps, as has been recognized by other researchers.[57,66,67] When the term of $\mathbf{E_\alpha}$ becomes dominant, it is a sign of a change in the limiting step of the reaction.

The estimated kinetics parameters by the actual method are called "effective", "apparent", "empirical", or "global" values of $E_{a,\alpha}$ and $\ln A_\alpha$. The effective parameters most likely, are composite values, determined by the sum of kinetic parameters of the involved individual steps assuming that the water delivery has the Arrhenius temperature dependency.[59,68] Global kinetic parameters differ from intrinsic parameters; they can vary strongly with the temperature and the extent of conversion [68–70] or take on negative values.[71] Such discrepancies are not expected for the $\mathbf{E_a}$ values of a single-step chemical reaction or a simple physical change. The relative constant values of kinetic parameters at the extent of α ≤ 0.4 are an indication of a single change: the vaporization of water below its boiling point with a very low barrier of energy [$\langle E_a \rangle$ = 23 ± 2 kJmol^{-1} Fig. 5(a)], smaller than the value of the heat of vaporization of water at similar vapor pressure (~ 45 kJmol^{-1}). Therefore, the E_a obtained in this work is related to the self-release of water from CDAAG during the experiment. The sudden decrease (~ 50%) in the energy barrier at the values of α larger than 0.4, is due to two factors, the hydrophobicity of the system and available energy at higher temperatures (above 50 °C).

The values of the pre-exponential factor ($\ln\mathbf{A}$) of DHGAA are in the range of 10 to 11,000 min^{-1} with the highest values at the α being 0.1 an 0.2, the beginning of dehydration, as shown in Fig 5 (b). The lowest values of $\mathbf{A}$ are indications of the physical changes in the system, which was the release of water by DAAG. The values of A for chemical reactions are above 10^6

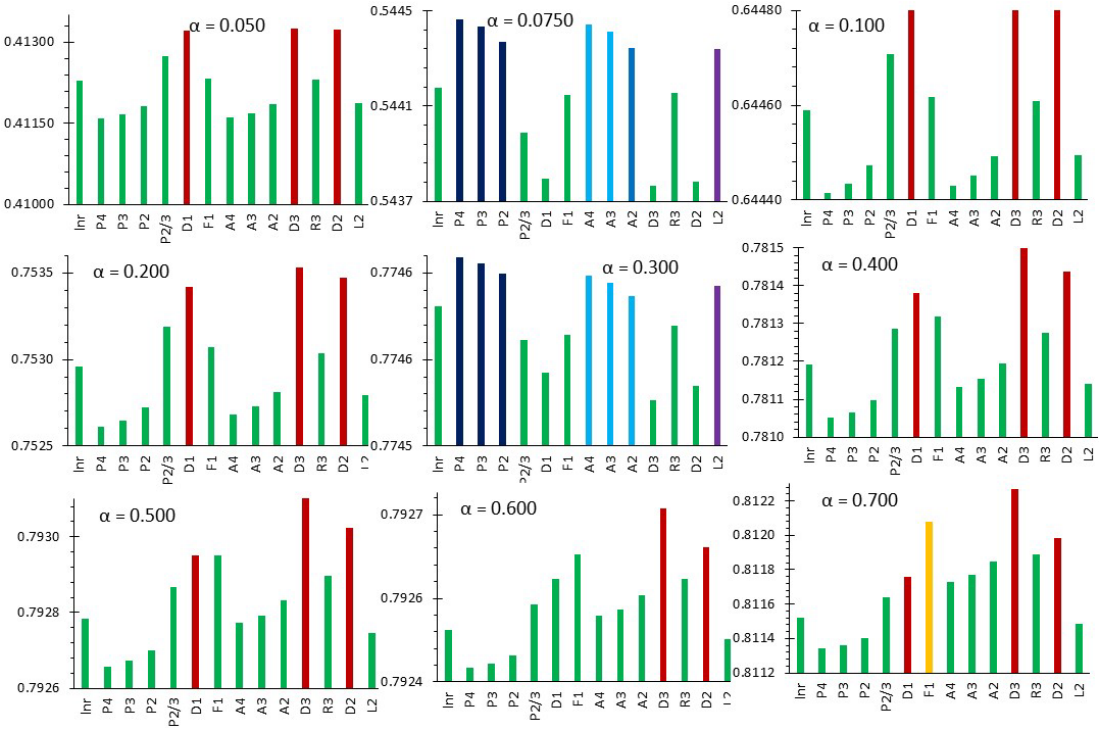

Fig. 6. Comparison of the values of r^2 of each $f(\alpha)$ (Table 1) at the indicated values of α

Each plot in Figure 6 compares the variation of the values of the correlations ($\mathbf{r^2}$) obtained by the application of 14 pre-assumed $f(\alpha)$ models for the indicated αvalue. The best-fitted model must show the highest value of $\mathbf{r^2}$, and it belongs to the diffusion-reaction models (D1, D3, and D3 shown in red) indicating the water release was taking place by diffusion from the hydrogel as expected. There were a few exceptions at the α values at 0.075 and 0.30 which the power law models fit better than diffusional models. Therefore, the release of water from CDAAG was by its diffusion and vaporization through CDAAG pore sites. The least-square fitting correlation was very low at the start and end of the process; it has a fair relative constancy in the range of **α** 0.20 to 0.75. However, judging the mechanism of dehydration by the best-fitted model to the experimental data must go with the circumstances regarding to process. Knowing that the water release mechanism involves several consecutive reactions, and the method catches only the rate-determining step of the reaction, which is the slowest one. Also, it was assumed that the temperature dependence of the mass loss due to the water release can be described by the Arrhenius relationship, and the hypothetical models of the reaction mechanism, $f(\alpha)$. The kinetic triplets were determined by first selecting a rate equation and then fitting it to the experimental data. The accuracy of the results depends on the adequateness of the chosen model to describe the process. As a result, the meaningful interpretability of the determined triplets depends on whether the selected rate equation adequately captures the essential features of the process mechanism, not the precise fit to the data. In this case, the diffusion models that described the sigmoidal nature of water release were the best fitting to the experimental data and the most meaningful for the process of releasing water from CDAAG.

IV. CONCLUSIONS, AND REMARKS

The water release mechanism involves multiple consecutive reactions, with the method focusing on the slowest step, known as the rate-determining step. To understand the dehydration mechanism, we consider both the experimental conditions and the best-fitting model for their data. We assumed that the temperature-dependent mass loss due to water release follows the Arrhenius relationship and explored various hypothetical reaction mechanism models represented as $f(\alpha)$.

To determine the kinetic parameters, we selected a rate equation and fitted it to experimental data. The accuracy of our results depends on how well the chosen model captures the process, rather than achieving a perfect fit to the data. In this study, diffusion models that described the sigmoidal nature of water release were found to be the best fit for the experimental data and provided meaningful insights into the process of releasing water from CDAAG.

Nine extents of water release reaction of CDAAG (**α**) were studied according to the pseudo-single component model of the isoconversional method by constructing the Arrhenius plot for each of them. The results showed a relative constancy of the activation energy ($\mathbf{E_a}$) within the range of **α** from 0.050 to 0.40, which indicated

a single change, i.e., the vaporization of water during the experiment. The average values of $\mathbf{E_a}$ in this range were found to be 24 ± 1 kJmol^{-1}, which is lower than the heat of vaporization of water under saturated vapor pressure. The best model to fit the experimental data was the diffusion model ranging the values of α from 0.05 to 0.7, except for the values of $\alpha = 0.075$ and 0.30 where the power-law models were fitting better.

The study shows that the maximum rate of water desorption depended on the heating rate. The highest rate of water generation at the heating rate of 0.25 Kmin^{-1} occurred at 39 °C, and at 4 Kmin^{-1}, it was at 98 °C, due to thermal lag effects. The DSC transition was observed around 35 °C, coinciding with the maximum water desorption rate when the value of $\beta = 0.25$ Kmin^{-1}. DSC transition confirmed that the release of water by CDAAG was facilitated by its structural transition from a hydrophilic to a hydrophobic state. These properties suggest that CDAAG is a promising water condenser for the construction of AWG.

ACKNOWLEDGEMENTS

The author acknowledges the support of the United States Department of Agriculture (USDA), National Institute of Food and Agriculture, Evans-Allen project number SCX-311-29-21. Also, we express our gratitude to Dr. Judith Salley, Dr. Louis Whitesides, and their teams for their constant encouragement and support. Any opinions, findings, conclusions, or recommendations expressed in this material are those of the authors and do not necessarily reflect those of the Funding Agency.

Bibliographic References

[1]. Li, R.; Shi, Y.; Alsaedi, M.; Wu, M.; Shi, L.; Wang, P. Hybrid Hydrogel With High Water Vapor Harvesting Capacity For Deployable Solar-Driven Atmospheric Water Generator. 2018, 52 (19), 11367–11377. Https://Doi.Org/10.1021/Acs.Est.8b02852.

[2]. Gou, X.; Guo, Z. Hybrid Hydrophilic-Hydrophobic CuO@TiO_2-Coated Copper Mesh For Efficient Water Harvesting. Langmuir 2020, 36 (1), 64–73. Https://Doi.Org/10.1021/Acs.Langmuir.9b03224.

[3]. Jarimi, H.; Powell, R.; Riffat, S. Review of Sustainable Methods for Atmospheric Water Harvesting. International Journal Of Low-Carbon Technologies. Oxford University Press May 1, 2020, Pp 253–276. Https://Doi.Org/10.1093/Ijlct/Ctz072.

[4]. Gleick, P. H.; Cohen, M.; Cooley, H.; Donnelly, K.; Fulton. Julian; Ha, M.-L.; Morrison, J.; Phurisamban, R.; Rippman, H.; Woodward, S. The World's Water Volume 9: The Report On Freshwater Resources; 2018.

[5]. Meza, I.; Siebert, S.; Döll, P.; Kusche, J.; Herbert, C.; Eyshi Rezaei, E.; Nouri, H.; Gerdener, H.; Popat, E.; Frischen, J.; Naumann, G.; Vogt, J. V.; Walz, Y.; Sebesvari, Z.; Hagenlocher, M. Global-Scale Drought Risk Assessment For Agricultural Systems. Natural Hazards And Earth System Sciences 2020, 20 (2), 695–712. Https://Doi.Org/10.5194/Nhess-20-695-2020.

[6]. Boretti, A.; Rosa, L. Reassessing The Projections Of The World Water Development Report. NPJ Clean Water 2019, 2 (1), 15. Https://Doi.Org/10.1038/S41545-019-0039-9.

[7]. Ciampi, M. 'Water Divide' In The Global Risk Society. International Review Of Sociology 2013, 23 (1), 243–260. Https://Doi.Org/10.1080/03906701.2013.771468.

[8]. Zhou, X.; Lu, H.; Zhao, F.; Yu, G. Atmospheric Water Harvesting: A Review Of Material And Structural Designs; American Chemical Society, 2020; Vol. 2, Pp 671–684. Https://Doi.Org/10.1021/Acsmaterialslett.0c00130.

[9]. Rubin, S. J. Water Costs And Affordability In The United States: 1990 To 2015. J Am Water Works Assoc 2018, 110 (4), 48–52. Https://Doi.Org/10.1002/Awwa.1062.

[10]. Spicer, N.; Parlee, B.; Chisaakay, M.; Lamalice, D. Drinking Water Consumption Patterns: An Exploration Of Risk Perception And Governance In Two First Nations Communities. Sustainability 2020, 12 (17), 6851. Https://Doi.Org/10.3390/Su12176851.

[11]. FAO. The State Of The World's Land And Water Resources For Food And Agriculture – Systems At Breaking Point (SOLAW 2021); FAO, 2021. Https://Doi.Org/10.4060/Cb7654en.

[12]. Fresán, U.; Marrin, D.; Mejia, M.; Sabaté, J. Water Footprint Of Meat Analogs: Selected Indicators According To Life Cycle Assessment. Water (Basel) 2019, 11 (4), 728. Https://Doi.Org/10.3390/W11040728.

[13]. Mekonnen, M. M.; Gerbens-Leenes, W. The Water Footprint Of Global Food Production. Water (Basel) 2020, 12 (10), 2696. Https://Doi.Org/10.3390/W12102696.

[14]. Vanham, D.; Mekonnen, M. M. The Scarcity-Weighted Water Footprint Provides Unreliable Water Sustainability Scoring. 2021, 756, 143992. Https://Doi.Org/10.1016/J.Scitotenv.2020.143992.

[15]. D. Mahan; O. Waissbluth; D. Caceres. Carcinogenic And Non-Carcinogenic Health Risks Of Arsenic Exposure In Drinking Water In The Rural Environment. Global J. Environ. Sci. Manage. 2020, 6 (2), 165–174.

[16]. (16) Guo, Y.; Zhou, X.; Zhao, F.; Bae, J.; Rosenberger, B.; Yu, G. Synergistic Energy Nanoconfinement and Water Activation in Hydrogels for Efficient Solar Water Desalination. ACS Nano 2019, 13 (7), 7913–7919. https://doi.org/10.1021/acsnano.9b02301.

[17]. Xu, J.; Zhang, J.; Fu, B.; Song, C.; Shang, W.; Tao, P.; Deng, T. All-Day Freshwater Harvesting through Combined Solar-Driven Interfacial Desalination and Passive Radiative Cooling. ACS Appl Mater Interfaces 2020, 12 (42), 47612–47622. https://doi.org/10.1021/acsami.0c14773.

[18]. Mekonnen, M. M.; Hoekstra, A. Y. Four Billion People Facing Severe Water Scarcity. Sci Adv 2016, 2 (2). https://doi.org/10.1126/sciadv.1500323.

[19]. Pérez-González, A.; Urtiaga, A. M.; Ibáñez, R.; Ortiz, I. State of the Art and Review on the Treatment Technologies of Water Reverse Osmosis Concentrates. Water Res 2012, 46 (2), 267–283. https://doi.org/10.1016/j.watres.2011.10.046.

[20]. Khalil, B.; Adamowski, J.; Shabbir, A.; Jang, C.; Rojas, M.; Reilly, K.; Ozga-Zielinski, B. A Review: Dew Water Collection from Radiative Passive Collectors to Recent Developments of Active Collectors. Sustain Water Resour Manag 2016, 2 (1), 71–86. https://doi.org/10.1007/s40899-015-0038-z.

[21]. Azeem, M.; Noman, M. T.; Wiener, J.; Petru, M.; Louda, P. Structural Design of Efficient Fog Collectors: A Review. Environ Technol Innov 2020, 20, 101169. https://doi.org/10.1016/j.eti.2020.101169.

[22]. Siddiqui, M. A.; Azam, M. A.; Khan, M. M.; Iqbal, S.; Khan, M. U.; Raffat, Y. Current Trends on Extraction of Water from Air: An Alternative Solution to Water Supply. International Journal of Environmental Science and Technology 2022. https://doi.org/10.1007/s13762-022-03965-8.

[23]. Hamidi, N.; Gargallo, L.; Whitesides, L. Water and Atmospheric Water Generation in Recent Progress in Science and Technology Vol. 5; Afefy, Prof. H. M., Ed.; B P International (a part of Sciencedomain International), 2023; Vol. 5, pp 43–67. https://doi.org/10.9734/bpi/rpst/v5.

[24]. Zhang, Y.; Zhu, W.; Zhang, C.; Peoples, J.; Li, X.; Felicelli, A. L.; Shan, X.; Warsinger, D. M.; Borca-Tasciuc, T.; Ruan, X.; Li, T. Atmospheric Water Harvesting by Large-Scale Radiative Cooling Cellulose-Based Fabric. Nano Lett 2022, 22 (7), 2618–2626. https://doi.org/10.1021/acs.nanolett.1c04143.

[25]. Anderson, P. J.; Miller, A. D.; O'malley, K. A.; Ceridon, M. L.; Beck, K. C.; Wood, C. M.; Wiste, H. J.; Mueller, J. J.; Johnson, J. B.; Johnson, B. D. Incidence and Symptoms of High Altitude Illness in South Pole Workers: Antarctic Study of Altitude Physiology (ASAP). Clin Med Insights Circ Respir Pulm Med 2011, 5, CCRPM.S6882. https://doi.org/10.4137/CCRPM.S6882.

[26]. Cashman, S.; Ma, C. (Xin); Garland, J.; Morelli, B. Overview of Resource Recovery-Based Sustainable Water Systems: Life Cycle Assessment Updates from US EPA's Safe and Sustainable Water Research Program; 2018. https://pasteur.epa.gov/uploads/10.23719/1503094/AWG_LCA_Report_Final_1.29.19.pdf (accessed 2023-04-02).

[27]. Ma, X.; Zhao, X.; Zhang, Y.; Liu, K.; Yang, H.; Li, J.; Akhlaghi, Y. G.; Liu, H.; Han, Z.; Liu, Z. Combined Rankine Cycle and Dew Point Cooler for Energy Efficient Power Generation of the Power Plants - A Review and Perspective Study. Energy 2022, 238, 121688. https://doi.org/10.1016/j.energy.2021.121688.

[28]. Park, H.; Haechler, I.; Schnoering, G.; Ponte, M. D.; Schutzius, T. M.; Poulikakos, D. Enhanced Atmospheric Water Harvesting with Sunlight-Activated Sorption Ratcheting. ACS Appl Mater Interfaces 2022, 14 (1), 2237–2245. https://doi.org/10.1021/acsami.1c18852.

[29]. Xi, Z.; Li, S.; Yu, L.; Yan, H.; Chen, M. All-Day Freshwater Harvesting by Selective Solar Absorption and Radiative Cooling. ACS Appl Mater Interfaces 2022, 14 (22), 26255–26263. https://doi.org/10.1021/acsami.2c05409.

[30]. Liu, X.; Beysens, D.; Bourouina, T. Water Harvesting from Air: Current Passive Approaches and Outlook; American Chemical Society, 2022; Vol. 4, pp 1003–1024. https://doi.org/10.1021/acsmaterialslett.1c00850.

[31]. Echeverria, C.; Fernandes, S.; Godinho, M.; Borges, J.; Soares, P. Functional Stimuli-Responsive Gels: Hydrogels and Microgels. Gels 2018, 4 (2), 54. https://doi.org/10.3390/gels4020054.

[32]. Banerjee, D.; Dedmon, H.; Rahmani, F.; Pasquinelli, M.; Ford, E. Cyclization Kinetics of Gel-spun Polyacrylonitrile/Aldaric-acid Sugars Using the Isoconversional Approach. J Appl Polym Sci 2022, 139 (11), 51781. https://doi.org/10.1002/app.51781.

[33]. Bertrand, T.; Peixinho, J.; Mukhopadhyay, S.; MacMinn, C. W. Dynamics of Swelling and Drying in a Spherical Gel. Phys Rev Appl 2016, 6 (6), 064010. https://doi.org/10.1103/PhysRevApplied.6.064010.

[34]. Zhao, F.; Zhou, X.; Liu, Y.; Shi, Y.; Dai, Y.; Yu, G. Super Moisture-Absorbent Gels for All-Weather Atmospheric Water Harvesting. Advanced Materials 2019, 31 (10), 1806446. https://doi.org/10.1002/adma.201806446.

[35]. Lu, H.; Shi, W.; Zhang, J. H.; Chen, A. C.; Guan, W.; Lei, C.; Greer, J. R.; Boriskina, S. V.; Yu, G. Tailoring the Desorption Behavior of Hygroscopic Gels for Atmospheric Water Harvesting in Arid Climates. Advanced Materials 2022, 34 (37), 2205344. https://doi.org/10.1002/adma.202205344.

[36]. Kim, S.; Choi, H. Switchable Wettability of Thermoresponsive Core–Shell Nanofibers for Water Capture and Release. ACS Sustain Chem Eng 2019, 7 (24), 19870–19879. https://doi.org/10.1021/acssuschemeng.9b05273.

[37]. Diouf, D.; Darmanin, T.; Diouf, A.; Dieng, S. Y.; Guittard, F. Surface Nanostructuration and Wettability of Electrodeposited Poly(3,4-Ethylenedioxypyrrole) and Poly(3,4-Propylenedioxypyrrole) Films Substituted by Aromatic Groups. ACS Omega 2018, 3 (7), 8393–8400. https://doi.org/10.1021/acsomega.8b00871.

[38]. Thakur, N.; Sargur Ranganath, A.; Sopiha, K.; Baji, A. Thermoresponsive Cellulose Acetate-Poly(N-Isopropylacrylamide) Core-Shell Fibers for Controlled Capture and Release of Moisture. ACS Appl Mater Interfaces 2017, 9 (34), 29224–29233. https://doi.org/10.1021/acsami.7b07559.

[39]. Hamidi, N.; Zhu, T. Characterization of Amphiphilic Cobaltocenium Copolymers via Size Exclusion Chromatography with Online Laser-Light Scattering and Viscometric Detectors. Journal of Macromolecular Science, Part B 2021, 60 (1), 30–50. https://doi.org/10.1080/00222348.2020.1819600.

[40]. Wei, M.; Gao, Y.; Li, X.; Serpe, M. J. Stimuli-Responsive Polymers and Their Applications. Polym Chem 2017, 8 (1), 127–143. https://doi.org/10.1039/C6PY01585A.

[41]. Guo, Y.; Bae, J.; Fang, Z.; Li, P.; Zhao, F.; Yu, G. Hydrogels and Hydrogel-Derived Materials for Energy and Water Sustainability. Chemical Reviews. American Chemical Society August 12, 2020, pp 7642–7707. https://doi.org/10.1021/acs.chemrev.0c00345.

[42]. Hanikel, N.; Prévot, M. S.; Yaghi, O. M. MOF Water Harvesters. Nat Nanotechnol 2020, 15 (5), 348–355. https://doi.org/10.1038/s41565-020-0673-x.

[43]. Nguyen, H. L.; Gropp, C.; Hanikel, N.; Möckel, A.; Lund, A.; Yaghi, O. M. Hydrazine-Hydrazide-Linked Covalent Organic Frameworks for Water Harvesting. ACS Cent Sci 2022. https://doi.org/10.1021/acscentsci.2c00398.

[44]. Kallenberger, P. A.; Fröba, M. Water Harvesting from Air with a Hygroscopic Salt in a Hydrogel–Derived Matrix. Commun Chem 2018, 1 (1), 28. https://doi.org/10.1038/s42004-018-0028-9.

[45]. Yilmaz, G.; Meng, F. L.; Lu, W.; Abed, J.; Peh, C. K. N.; Gao, M.; Sargent, E. H.; Ho, G. W. Autonomous Atmospheric Water Seeping MOF Matrix. Sci Adv 2020, 6 (42). https://doi.org/10.1126/sciadv.abc8605.

[46]. Díaz-Marín, C. D.; Zhang, L.; Lu, Z.; Alshrah, M.; Grossman, J. C.; Wang, E. N. Kinetics of Sorption in Hygroscopic Hydrogels. Nano Lett 2022, 22 (3), 1100–1107. https://doi.org/10.1021/acs.nanolett.1c04216.

[47]. Flory, P. J. Principles of Polymer Chemistry; Cornell University Press: Ithaca, NY, , 1953.

[48]. LaPotin, A.; Kim, H.; Rao, S. R.; Wang, E. N. Adsorption-Based Atmospheric Water Harvesting: Impact of Material and Component Properties on System-Level Performance. Acc Chem Res 2019, 52 (6), 1588–1597. https://doi.org/10.1021/acs.accounts.9b00062.

[49]. Gido, B.; Friedler, E.; Broday, D. M. Liquid-Desiccant Vapor Separation Reduces the Energy Requirements of Atmospheric Moisture Harvesting. Environ Sci Technol 2016, 50 (15), 8362–8367. https://doi.org/10.1021/acs.est.6b01280.

[50]. Mulchandani, A.; Edberg, J.; Herckes, P.; Westerhoff, P. Seasonal Atmospheric Water Harvesting Yield and Water Quality Using Electric-Powered Desiccant and Compressor Dehumidifiers. Science of The Total Environment 2022, 825, 153966. https://doi.org/10.1016/j.scitotenv.2022.153966.

[51]. Mehta, J. R.; Desai, T. K.; Patel, A. K.; Diyora, H. B.; Rabadiya, A. S. Preliminary Investigations on a Novel Rotating Media Liquid-Air Contacting Device without Liquid Pool. In Energy Procedia; Elsevier Ltd, 2017; Vol. 109, pp 167–173. https://doi.org/10.1016/j.egypro.2017.03.088.

[52]. Entezari, A.; Ejeian, M.; Wang, R. Super Atmospheric Water Harvesting Hydrogel with Alginate Chains Modified with Binary Salts. ACS Mater Lett 2020, 2 (5), 471–477. https://doi.org/10.1021/acsmaterialslett.9b00315.

[53]. Liu, X.; Wang, X.; Kapteijn, F. Water and Metal-Organic Frameworks: From Interaction toward Utilization. Chemical Reviews. American Chemical Society August 26, 2020, pp 8303–8377. https://doi.org/10.1021/acs.chemrev.9b00746.

[54]. Feng, R.; Xu, C.; Song, F.; Wang, F.; Wang, X.-L. L.; Wang, Y.-Z. Z. A Bioinspired Slippery Surface with Stable Lubricant Impregnation for Efficient Water Harvesting. 2020, 12 (10), 12373–12381. https://doi.org/10.1021/acsami.0c00234.

[55]. Zhu, S.-Q.; Feng, R.; Liang, Z.-H.; Wang, X.-L.; Wang, Y.-Z.; Song, F. Efficient Water Harvesting Enabled by Porous Architecture-Containing Hybrid Surfaces. Ind Eng Chem Res 2022. https://doi.org/10.1021/acs.iecr.2c00717.

[56]. Aleid, S.; Wu, M.; Li, R.; Wang, W.; Zhang, C.; Zhang, L.; Wang, P. Salting-in Effect of Zwitterionic Polymer Hydrogel Facilitates Atmospheric Water Harvesting. ACS Mater Lett 2022, 4 (3), 511–520. https://doi.org/10.1021/acsmaterialslett.1c00723.

[57]. Ding, J.; Zhang, X.; Hu, D.; Ye, S.; Jiang, J. Model-Free Kinetic Determination of Pre-Exponential Factor and Reaction Mechanism in Accelerating Rate Calorimetry. Thermochim Acta 2021, 702, 178983. https://doi.org/10.1016/j.tca.2021.178983.

[58]. Perejón, A.; Sánchez-Jiménez, P. E.; Criado, J. M.; Pérez-Maqueda, L. A. Kinetic Analysis of Complex Solid-State Reactions. A New Deconvolution Procedure. J Phys Chem B 2011, 115 (8), 1780–1791. https://doi.org/10.1021/jp110895z.

[59]. Pérez-Maqueda, L. A.; Criado, J. M.; Sánchez-Jiménez, P. E. Combined Kinetic Analysis of Solid-State Reactions: A Powerful Tool for the Simultaneous Determination of Kinetic Parameters and the Kinetic Model without Previous Assumptions on the Reaction Mechanism. J Phys Chem A 2006, 110 (45), 12456–12462. https://doi.org/10.1021/jp064792g.

[60]. Hamidi, N. Upcycling Poly(Vinyl Chloride) Waste Tubes: Studies of Thermal Stability and Kinetics of Films Made of Waste Polyvinylchloride Tube at the Initial Steps of Degradation. J Appl Polym Sci 2023, 140 (13). https://doi.org/10.1002/app.53663.

[61]. Hamidi, N.; Yazdani-Pedram, M.; Abdussalam, N. Upcycling Poly(Ethylene Terephthalate) Wastes by Solvent Extraction: Thermal Stability and Kinetics Studies of the Recovered <scp>PET</Scp>. J Appl Polym Sci 2022, 139 (14), 51905. https://doi.org/10.1002/app.51905.

[62]. Hamidi, N.; Williams, I.; Hamidi, H. Kinetics of the Water Release of Hygroscopic Acrylamide Gel Embedded in Calcium Chloride by Thermogravimetric Analysis. Global Journal of Science Frontier Research 2023, 1–11. https://doi.org/10.34257/GJSFRHVOL23IS3PG1.

[63]. Nasrollah Hamidi; Mehrdad Yazadani-Pedram . Water Release Kinetics of Hygroscopic Acrylamide Enbibed in CaCl2 by Thermogravimetric and Differential Scanning Calorimetry Methods. Journal of Materials Science Research and Reviews 2023, 6 (4), 655–659.

[64]. Ozawa, T. Controlled Rate Thermogravimetry: New Usefulness of Controlled Rate Thermogravimetry revealed by Decomposition of Polyimide. J Therm Anal Calorim 2000, 59 (1/2), 375–384. https://doi.org/10.1023/A:1010125121227.

[65]. Park, H.-J. Evaluation of the Activation Energy of Chlorinated Poly Vinyl Chloride (CPVC) Using Thermogravimetric Analysis. Fire science and engineering 2019, 33 (1), 1–6. https://doi.org/10.7731/kifse.2019.33.1.001.

[66]. Sbirrazzuoli, N. Advanced Isoconversional Kinetic Analysis for the Elucidation of Complex Reaction Mechanisms: A New Method for the Identification of Rate-Limiting Steps. Molecules 2019, 24 (9), 1683. https://doi.org/10.3390/molecules24091683.

[67]. Sbirrazzuoli, N. Determination of Pre-Exponential Factors and of the Mathematical Functions f(α) or G(α) That Describe the Reaction Mechanism in a Model-Free Way. Thermochim Acta 2013, 564, 59–69. https://doi.org/10.1016/j.tca.2013.04.015.

[68]. Vyazovkin, S.; Burnham, A. K.; Favergeon, L.; Koga, N.; Moukhina, E.; Pérez-Maqueda, L. A.; Sbirrazzuoli, N. ICTAC Kinetics Committee Recommendations for Analysis of Multi-Step Kinetics. Thermochim Acta 2020, 689, 178597. https://doi.org/10.1016/j.tca.2020.178597.

[69]. Peterson, J. D.; Vyazovkin, S.; Wight, C. A. Kinetics of the Thermal and Thermo-Oxidative Degradation of Polystyrene, Polyethylene and Poly(Propylene); 2001; Vol. 202.

[70]. Dong, Z.; Yang, Y.; Cai, W.; He, Y.; Chai, M.; Liu, B.; Yu, X.; Banks, S. W.; Zhang, X.; Bridgwater, A. V.; Cai, J. Theoretical Analysis of Double Logistic Distributed Activation Energy Model for Thermal Decomposition Kinetics of Solid Fuels. Ind Eng Chem Res 2018, 57 (23), 7817–7825. https://doi.org/10.1021/acs.iecr.8b01527.

[71]. Atkins, P.; De Paula, J. Physical Chemistry, 9th Edition , 9th ed.; W. H. Freeman, 2009: New York, NY, 2009.